Channel-specific dielectronic recombination of highly charged krypton

T. Fuchs, C. Biedermann, and R. Radtke
Max-Planck-Institut für Plasmaphysik, Bereich Plasmadiagnostik, EURATOM Association, D-10117 Berlin, Germany

E. Behar and R. Doron
Racah Institute of Physics, The Hebrew University, 91904 Jerusalem, Israel
(Received 26 May 1998)

We have measured the channel-specific cross sections for dielectronic recombination (DR) via the KLn $(n=2,\ldots,5)$ resonance series of He-, Li-, and Be-like krypton ions. The measurements were made with an electron beam ion trap, and the DR cross sections were determined relative to the cross section for nonresonant radiative recombination. In the present electron-beam ion-trap experiment, up to five charge states (He- to C-like krypton) were detected in the trap. A fit procedure was used to compare the experimental data with theoretical calculations. The results agree well with the predictions. Additionally, the radiative relaxation mechanism following the stabilization transition in the dielectronic-recombination process was analyzed. The experimental approach used for measuring the DR excitation function opens up a spectroscopic method for the determination of the relative abundance of the highly charged ions. [S1050-2947(98)01512-1]

PACS number(s): 34.80.Kw, 34.80.Dp, 52.25.Nr

I. INTRODUCTION

Dielectronic recombination (DR) is an important atomic process in high-temperature laboratory and astrophysical plasmas and has initiated many theoretical and experimental studies. In the usual two-step schematic picture, dielectronic recombination is described as the resonant capture of a free electron by an ion, thereby forming a doubly excited intermediate state. If the intermediate state thus created decays to a nonautoionizing state by the emission of a stabilizing photon, the DR process is complete. Schematically, for a He-like ground-state target ion, dielectronic recombination is given as

$$1s^2+e\rightarrow 1snln'l'\begin{cases}\nearrow & 1s^2nl+h\nu_1\\ \searrow & 1s^2n'l'+h\nu_2.\end{cases} \qquad (1)$$

It is essential for the present channel-specific investigation that the intermediate state $1snln'l'$ has, for $n<n'$, two channels available to which it can decay. For the KLM resonance $(n=2,\ n'=3)$, for example, the DR capture gives rise to radiative *stabilizing* transitions where $n=2-1$ or $n=3-1$ x rays are emitted. If electron capture into the N shell and concurrent excitation of the $1s$ electron to the L shell (or vice versa) takes place (KLN resonance), the recombined ion can stabilize via $n=2-1$ or $n=4-1$ transitions, etc. In addition, if a $n=2-1$ transition has occurred for the KLN resonance, the subsequent decay of the spectator N-shell electron leads to *relaxation* transitions, which produce either $n=4-2$ or $n=4-3$ and $n=3-2$ x rays, depending on the branching ratio of the ion under consideration.

From x-ray spectroscopic measurements of the DR process (1) which distinguish between the different stabilizing transitions, channel-specific dielectronic recombination cross sections can be obtained. Channel-specific measurements reveal more details of the dielectronic resonances and indicate what fraction of radiative stabilization proceeds via which of the competing decay channels. It is also important to stress that, when compared to calculations, such measurements result in a more stringent test of theoretical predictions than do measurements of total cross sections.

In this paper, we report on a measurement of the DR cross sections for the KLL, KLM, KLN, and KLO resonances of highly charged krypton ions that is channel specific. Our measurement was performed at the Berlin electron beam ion trap (EBIT) facility [1] using EBIT's capability to scan the electron-beam energy linearly through the dielectronic-recombination resonances. The experimental cross sections were obtained from the characteristic x rays emitted in the DR process following the procedure described in Ref. [2] for comparing the observed dielectronic-excitation function to theory. For this comparison, theoretical values of the dielectronic-resonance strengths and the radiative-recombination (RR) cross sections are required. We have evaluated these data from atomic-structure calculations using the HULLAC computer code package [3].

Krypton was chosen since it has been recently proposed as a coolant for the plasma edge region of future tokamaks, such as the International Thermonuclear Experimental Reactor (ITER) [4]. In addition, for ITER plasmas, krypton is the most likely candidate for Doppler broadening measurements to determine the central ion temperature [5,6]. In order to predict the effect of injected krypton on the ITER performance and explore its benefit for diagnostic applications, accurate atomic physics data will be needed, including transition energies and line intensities as well as cross sections for ionization and recombination.

II. EXPERIMENT

The EBIT technique [7] employs a monoenergetic 70-μm-diameter electron beam, which is formed by accelerating and guiding electrons from an electron gun into the trap.The trap consists of an assembly with three drift tubes. Atoms or low-charged ions injected into the trap are ionized by multiple electron collisions and radially confined by the

space charge of the electron beam. Axial confinement is provided within a 2-cm-long trapping region by the two end-drift tubes, which are biased positive with respect to the center-drift tube. For the present dielectronic-recombination measurements, neutral krypton atoms were continuously fed into the trap from a differentially pumped gas injector (pressure in the gas injector: 2.5×10^{-6} Pa). In order to limit the beam-energy spread to approximately 50 eV full width at half maximum (FWHM), a moderate beam current ($I_{\mathrm{beam}}=70$ mA) was applied. The high end of the charge state distribution is limited by the voltage applied to the drift tube. In order to optimize the run conditions of EBIT towards a high ratio of He-like to Li-like krypton ions, modeling calculations have been performed using the methods of Ref. [8]. From these calculations, appropriate values for the electron-beam energy, ionization time, and axial trap depth could be derived. However, by analyzing the measured dielectronic-excitation function, we inferred that the abundance of He-like krypton was no more than $40-50\%$ of all the Kr ions at best. This is less than predicted by the model, and we were not able to improve this percentage by choosing a different beam energy, trap depth, or pressure in the gas injector. We attribute these limitations to the effect of the neutral gas density, which, in fact, is difficult to control in EBIT due to the additional gas load from stray atoms in the halo of the gas flow from the gas injector. Neutral krypton atoms affect the population of the higher ion stages via charge-exchange recombination, and if the background gas pressure is high this can result in a dramatic shift of the steady-state ionization balance as was confirmed by our numerical studies.

To measure the characteristic DR lines from the different groups of KLn resonances, the following scheme was used: The electron-beam energy was first set to the ionization energy well away from the excitation energies for the individual resonances, which are around 9.0, 11.3, 12.1, and 12.4 keV, respectively. For example, to measure the KLM resonance, the ionization energy was set to 11.7 keV. After the ionization phase (which extended up to 2 s), the beam energy was switched from the ionization energy to a value just below the resonance under investigation. For each resonance, we have then performed linear energy sweeps where the beam energy was ramped through about 500 eV (sweep rate: $10-100$ eV/ms, depending on the particular resonance). This switch-sweep procedure was repeated every 150 ms for about 1.5 s, after which the trap was dumped and refilled with fresh ions. During the sweeps, we have measured the x rays emitted from the trapped ions using a solid-state detector. The detector (active diameter 6 mm; energy resolution: 135 eV at 5.9 keV) was mounted behind a 12.5-μm beryllium window resulting in a lower cutoff at about 1-keV x-ray energy steeply reducing the transmission within a small energy range. Data from the detector were stored in an analog-to-digital converter (ADC) and fed into a multichannel scaler (MCS). The MCS scan was triggered by an appropriate pulse generated at the start of each sweep of the beam energy. During the scan, the MCS recorded the event time for the measured x rays; the resolution (dwell time) was $5-50$ μs, depending on the sweep rate. The dump-sweep cycle was repeated numerous times, with the data from each scan being added to the previous scans. Combining the pulse-height spectrum from the ADC with the MCS data and using the wave form of the drift-tube voltage (which was recorded during each sweep), we could produce a plot of x-ray energy versus electron beam energy for the events observed.

A typical scatter plot taken with the electron-beam energy swept through the KLN dielectronic resonance is given in Fig. 1(a). The bright traces in the upper part correspond to the stabilizing transitions where $n=4-1$ and $n=2-1$ x rays are emitted in the DR process, respectively. As expected, the $n=2-1$ stabilizing transition involving the L-shell electron dominates the KLN resonance. It produces the x rays at about 13 keV while the alternative $n=4-1$ channel produces the x rays at about 16 keV. The traces in the lower part of Fig. 1(a) are associated with the $n=3-2$ transitions at about 2 keV and the $n=4-2$ transitions at about 3 keV. They arise from direct excitation as well as relaxation transitions of the N-shell spectator electron.

Figures 1(b) and 1(c) show the dielectronic-excitation functions for the $n=4-1$ and $n=2-1$ x rays, respectively. The excitation functions are different in magnitude and energy dependence, reflecting the distribution of the DR resonance states from the $1s2l4l'$ configurations and the different rates for the two channels to which these states can decay by stabilizing transitions. A particular aspect of our investigation is to observe not only the emission generated by the stabilizing part of the dielectronic-recombination process itself, but also the emission from the ion-relaxation process of the singly excited ion remaining thereafter. This ion relaxation is of importance in many respects to plasma physics and atomic theory and has been analyzed recently for highly charged barium [9]. Figures 1(d) and 1(e) show the excitation functions for the $n=4-2$ and $n=3-2$ relaxation transitions generated from the respective cuts marked in Fig. 1(a). The fraction of counts measured for the $n=4-2$ transition with respect to the $n=2-1$ counts is 81%, showing that most of the ion relaxation following an $n=2-1$ transition proceeds in one step. The alternative relaxation channel is when the $n=4$ population is shifted to the $n=2$ level via $n=4-3-2$ radiative cascades. The relatively low-energy $n=4-3$ x rays could not be observed here due to the detector cutoff at about 1 keV; however, the $n=3-2$ relaxation transitions are observed and could be separated from the underlying collisionally excited krypton spectra. The fraction of counts measured for these transitions is 13%, i.e., a total of 94% of the $n=2-1$ DR counts is detected also in the relaxation transitions.

In Sec. IV we present a more detailed analysis of our experimental results for the DR resonances, which is based on a theory-experiment comparison in terms of dielectronic-resonance strengths.

III. THEORY AND CALCULATION

The DR processes studied in the present experiment consist of a free electron captured by a highly ionized krypton atom (e.g., He-like) in the initial ground-state level i ($1s^2$) to form a (Li-like) ion in an intermediate autoionizing doubly excited level d ($1s2ln'l'$) followed by a radiative stabilization to a final level f ($1s^2n'l'$ or $1s^22l$) lying below the first ionization limit (i). For He-like target ions, these DR reactions are schematically represented by Eq. (1). In the light of

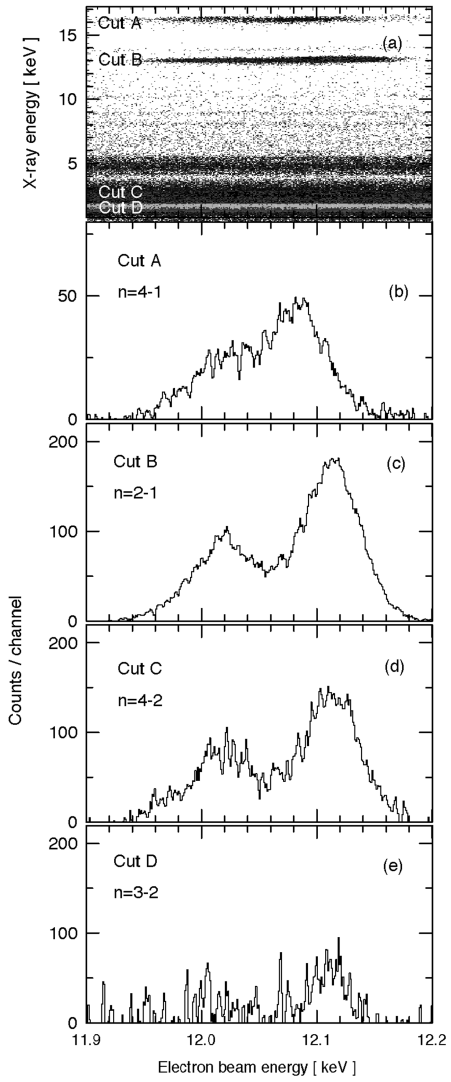

FIG. 1. Dielectronic-recombination spectrum and excitation functions for the KLN resonance of krypton. (a) Scatter plot of x-ray energy vs electron-beam energy. The values for the beam energy correspond to the drift-tube voltage corrected for the space charge in the trap. The broad trace at about 5 keV x-ray energy originates from an unavoidable minor barium background in the trap. (b)–(e) Excitation functions corresponding to the cuts *A*, *B*, *C*, and *D*, respectively. For the projections (b) and (c), representing $n=4-1$ and $n=2-1$ transitions, respectively, we have subtracted the detected background from nonresonant radiative recombination events. The projections (d) and (e) represent $n=4-2$ and $n=3-2$ relaxation transitions of the *N*-shell spectator electron following radiative stabilization. (d) and (e) were generated from the respective cuts *C* and *D* by subtracting the events from the collisionally excited background. Note that we have swept the beam energy through about 500 eV, which more than covers the KLN resonance; in this way, we could record and identify the direct excitation and radiative recombination counts, which appear in the resonance spectrum [see respective cuts *A* to *D* in (a)] as background.

the experimental difficulties to isolate the He-like krypton ions from ions in adjacent charge states, the investigation of the DR cross section for Li- and Be-like krypton ions is essential here as well. For these ions the analogous DR reactions are

$$1s^2 2s + e \rightarrow 1s2s2ln'l' \begin{cases} \nearrow & 1s^2 2s2l + h\nu_1 \\ \searrow & 1s^2 2sn'l' + h\nu_2 \end{cases} \tag{2}$$

and

$$1s^2 2s^2 + e \rightarrow 1s2s^2 2pn'l' \begin{cases} \nearrow & 1s^2 2s^2 2p + h\nu_1 \\ \searrow & 1s^2 2s^2 n'l' + h\nu_2, \end{cases} \tag{3}$$

respectively. Here, $h\nu_1$ and $h\nu_2$ are the energies of the x-ray photons to be detected in the stabilizing radiative transition. In order to fit the high-energy end of the DR cross section for the KLL resonance, it was necessary to include the B- and C-like krypton ions as well. The ground-state configuration of these ions are $1s^2 2s^2 2p$ and $1s^2 2s^2 2p^2$, respectively. Compared to He-, Li-, or Be-like ions, dielectronic recombination onto these systems involves many more doubly excited levels with the result that the DR spectrum is much more complex.

The natural width of the cross section $\sigma_{idf}^{\mathrm{DR}}(E)$ for DR from the initial level *i* through the intermediate level *d* to the final level *f* is about two orders of magnitude smaller than the beam-energy width of 50 eV FWHM. Thus, instead of working with the theoretical narrow profiled DR cross section, it is justified to characterize each DR resonance by the resonance strength, which is the cross section integrated over all energies. The resonance strength S_{idf} for DR from *i* through *d* to *f* is defined by

$$S_{idf} = \int_0^\infty \sigma_{idf}^{\mathrm{DR}}(E)\,dE = \frac{h^3}{8\pi m_e E_{di}} \frac{g_d A_{di}^a}{2g_i} \times \frac{A_{df}}{\sum_{i'} A_{di'}^a + \sum_{f'} A_{df'} + \sum_{d'} A_{dd'}} \tag{4}$$

where E_{di} is the capture-resonance energy, g_d and g_i are the multiplicities of levels *d* and *i*, respectively. A_{df} is the Einstein coefficient for spontaneous emission from level *d* to level *f*, and A_{di}^a is the coefficient for autoionization from level *d*, to level *i*. *h* is the Planck constant and m_e is the electron mass. The sums in the denominator of Eq. (4) are taken over all possible autoionization and radiative transitions from level *d*, including radiative cascades to lower doubly excited levels d'. More details on the methods for calculating DR cross sections and DR rate coefficients can be found in Ref. [10].

All the atomic data used in the present calculations are obtained by employing the multiconfiguration relativistic Hebrew University Lawrence Livermore Atomic Code (HULLAC) developed by Bar-Shalom *et al.* [3]. The intermediate-coupling detailed level energies are calculated using the relativistic version of the parametric potential method [11], including full configuration mixing. The radiative-decay and autoionization-rate coefficients are explicitly calculated from first-order perturbation theory. The autoionization coefficients are calculated in the distorted-wave approximation, implementing the highly efficient factorization-interpolation method [12]. As a preliminary step, the presently calculated total autoionization and radiative coefficients are compared to previously calculated data

TABLE I. The presently calculated (HULLAC) rate coefficients for autoinization and total rate coefficients for radiative decay from the $1s2ln'l'$ $(n'=2,3)$ doubly excited levels, compared to the (MCDF) results of Ref. [13]. The coefficients are given for the strongest DR channels only. $X[Y]$ stands for $X\cdot 10^{Y}$.

Config. and term	A_{di}^{a} (s^{-1})		$\Sigma A_{df'}+\Sigma A_{dd'}$ (s^{-1})	
	HULLAC	MCDF	HULLAC	MCDF
$1s2s^2\,{}^2S_{1/2}$	1.46[14]	1.59[14]	5.05[13]	5.11[13]
$1s2s(^3S)2p^2P_{1/2}$	7.85[13]	9.74[13]	6.80[14]	7.40[14]
$1s2s(^1S)2p^2P_{1/2}$	4.89[13]	4.58[13]	1.07[15]	9.79[14]
$1s2s(^1S)2p^2P_{3/2}$	1.10[14]	1.11[14]	1.84[13]	2.96[13]
$1s2p^2\,{}^4P_{5/2}$	7.11[13]	7.08[13]	3.50[14]	3.87[14]
$1s2p^2\,{}^2D_{3/2}$	1.23[14]	1.19[14]	1.45[15]	1.46[15]
$1s2p^2\,{}^2D_{5/2}$	9.91[13]	9.89[13]	5.26[14]	5.09[14]
$1s2p^2\,{}^2P_{3/2}$	4.75[13]	4.11[13]	2.08[15]	1.97[15]
$1s2p^2\,{}^2S_{1/2}$	3.13[13]	3.06[13]	1.00[15]	9.60[14]
$1s2s(^1S)3p^2P_{3/2}$	1.90[13]	1.90[13]	1.86[14]	1.82[14]
$1s2p(^3P)3s^2P_{1/2}$	4.61[13]	5.75[13]	3.31[14]	3.29[14]
$1s2p(^3P)3s^2P_{3/2}$	3.02[13]	3.18[13]	8.22[13]	9.41[13]
$1s2p(^3P)3p^4D_{5/2}$	1.13[13]	1.17[13]	3.15[14]	3.70[14]
$1s2p(^3P)3p^4P_{5/2}$	1.87[13]	1.91[13]	1.29[14]	1.41[14]
$1s2p(^1P)3p^2D_{3/2}$	3.58[13]	3.54[13]	1.58[15]	1.53[15]
$1s2p(^3P)3p^2D_{5/2}$	2.57[13]	2.81[13]	3.66[14]	3.30[14]
$1s2p(^1P)3p^2D_{5/2}$	1.95[13]	1.76[13]	1.63[15]	1.57[15]
$1s2p(^1P)3p^2P_{3/2}$	2.18[13]	1.86[13]	1.57[15]	1.51[15]
$1s2p(^1P)3d^2F_{7/2}$	1.28[13]	1.26[13]	1.36[15]	1.34[15]

published by Chen in a paper on dielectronic satellite spectra for He-like ions [13]. This paper includes only the relatively low-lying doubly excited Li-like levels $1s2ln'l'$ $(n'=2,\ 3)$. The data in Ref. [13] were obtained by using the multiconfiguration Dirac-Fock (MCDF) method, which is very different from the present HULLAC method. In Table I, the autoionization coefficients A_{di}^{a} and the total radiative coefficients $\Sigma A_{df'}+\Sigma A_{dd'}$ [appearing in Eq. (4)] calculated separately by both codes are given for the strongest $1s2ln'l'$ $(n'=2,\ 3)$ DR resonances. The configuration and term of each doubly excited level (d) are given in the first column. It is interesting to note that the $1s2s^2\,{}^2S_{1/2}$ level given in the first line in Table I has allowed radiative decays and thus is a significant DR channel only due to the mixing with the $1s2p^2$ configuration. It should also be pointed out that the only energetically allowed autoionization process from the $1s2ln'l'$ $(n'=2,3)$ Li-like levels is the autoionization to the $1s^2$ He-like ground state.

It can be seen from Table I that in almost all cases, the agreement between the results obtained using the HULLAC code and those obtained using the MCDF code is within about 15%. For the predominant transitions ($A_{di}^{a}>10^{14}\ s^{-1}$, $\Sigma A_{df}>10^{15}\ s^{-1}$), the discrepancies are even as small as a few percent only. It is important to point out that neither of the two codes gives consistently higher or lower coefficients with respect to the other one. Consequently, the agreement between the total DR effects calculated separately by both codes is found to be even better than the agreement between the results for particular transitions, such as those shown in Table I.

IV. ANALYSIS AND RESULTS

The procedure to obtain experimental DR resonance strengths is based on a comparison of measured and predicted dielectronic-excitation functions, determining the beam-energy resolution and the ionization balance simultaneously [2]. The observed dielectronic-recombination spectra were all normalized to the $n=2$ radiative-recombination photons, which were acquired when the electron-beam energy was swept through the off-resonance energies. With this procedure we determined the resonance strengths relative to the cross section for radiative recombination σ_{RR}. Values for σ_{RR} were obtained with the methods of Ref. [3], and we mention here that these data are deemed to be accurate within a 3% error limit [14].

In comparing the experimental results with theory, one has to account for the fact that radiation from EBIT is in general anisotropic. The reason is that collisions within the electron beam occur in a preferred direction, inducing an uneven population of the magnetic sublevels. As a result, the ensemble of the radiating ions has some degree of anisotropy, and intensities are then a function of the angle between the beam axis and the direction of observation [15]. In the present experiment we have observed the x rays at 90° to the beam direction. For electric-dipole radiation emitted during dielectronic recombination through level d to level f and observed at this particular angle, the angular correction factor W_{df} that accounts for the anisotropy is

$$W_{df}(90^\circ)=\frac{3}{3-P}, \tag{5}$$

where P is the degree of linear polarization [16]. Since electric-dipole radiation overwhelmingly dominates the DR process, we rely on this formula to determine the effect of angular distribution. P in Eq. (5) can be positive or negative, depending on the angular momenta J_i of the levels involved

in the transition. We have calculated W_{df} for a large number of individual resonances occurring in He- and Be-like krypton ions. For P we used the theoretical values obtained in Ref. [17] where the linear polarization was calculated for various typical DR lines. From our results, we infer that the stabilizing transitions with $\Delta J = J_d - J_f = 1$ contribute more than $60-70\%$ to the total strength of each of the resonance groups. The size of linear polarization associated with $\Delta J = 1$ transitions is at the $0.5-0.6$ level according to Ref. [17], which, in turn, gives $W_{df}(90°) = 1.20$ and 1.25, respectively. Thus, for the largest contribution to the dielectronic-recombination spectrum, we expect the x-ray emission intensity measured at 90° to be about $20-25\%$ stronger than in the case of isotropic emission. The majority of the remaining resonances with intermediate and small strengths produce x-ray lines that have negative polarizations or are unpolarized; the latter case corresponds to isotropic radiation. The average of the angular distribution correction $W_{df}(90°)$ for these lines is typically at the 0.9 level. Accordingly, for this $30-40\%$ fraction of the DR spectrum we expect the emission intensity to be reduced (relative to isotropic emission) by about 10%.

For radiative recombination (RR) of ions and electrons from a beam, it was established in recent theoretical calculations (see, e.g., Refs. [14] and [18]) that the cross section for the emission of x rays at 90° to the incident electron beam is generally larger than the spherical average. The angular factors that account for the anisotropic behavior of the total cross sections show major variations as a function of the electron energy, but are nearly independent of the ion species as demonstrated by Scofield [14] for He-like nickel and Ne-like barium. We have used the results of Ref. [14] to correct the RR cross sections obtained from the HULLAC code for the effect of angular distribution. For electrons in the 10–20 keV range, we assign a 23% correction for the RR cross section. This value is very close to the 20–25% intensity increase due to angular corrections predicted for the largest part of the dielectronic-recombination spectrum. Thus, if we normalize the DR x rays to the intensity of the photons emitted by RR to $n=2$, one can expect that the angular effects do largely compensate each other. Although the polarized and nonisotropic x-ray emission is an important feature of EBIT, the impact of the effect on the normalization procedure seems to be less significant. In fact, a more detailed estimate shows that neglecting it would add an uncertainty in the determination of the DR cross sections, which is no more than 7–10%. Since this value is relatively small, we decided to suppress any angular corrections in the fit procedure for the dielectronic-excitation functions.

The experimental data were fitted to the following function predicting the intensity ratio of I_{DR}, the number of photons remaining after the nonresonant background is subtracted from the observed dielectronic-excitation spectrum, and $I_{\mathrm{RR}(2)}$, the number of photons from radiative recombination to $n=2$:

$$\frac{I_{\mathrm{DR}}}{I_{\mathrm{RR}(2)}} = \frac{\sum_q x_q \sigma_i^{\mathrm{DR}}(q,E)}{\sum_q x_q \sigma_{\mathrm{RR}(2)}(q,E)}. \tag{6}$$

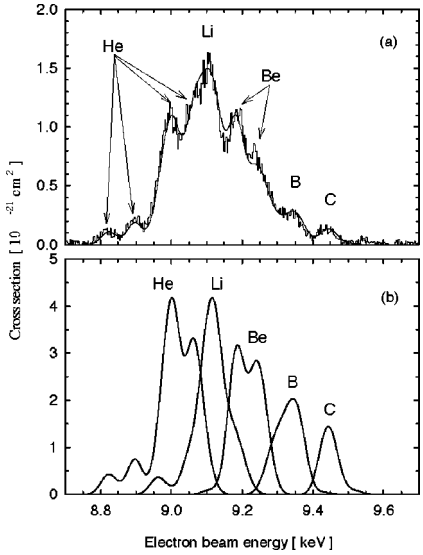

FIG. 2. (a) Experimental and theoretical DR cross sections for the KLL resonance of krypton target ions. The signatures of the He-, Li-, Be-, B-, and C-like charge states in the spectrum are marked. The relative charge-state balance determined through the fitting process is $x_{\mathrm{He}}=0.25$, $x_{\mathrm{Li}}=0.30$, $x_{\mathrm{Be}}=0.22$, $x_{\mathrm{B}}=0.14$, and $x_{\mathrm{C}}=0.09$. The width of the Gaussian electron-beam profile that provides a match to the observed dielectronic-excitation function is 50 eV. The area of the fit ($\Sigma S_{idf} = 3.8\times10^{-19}$ cm^2 eV) equals the area of the experimental spectrum to within 2%. Shown in (b) are the theoretical DR cross sections for the He-like to C-like charge states; the curves were obtained by applying a 50-eV FWHM Gaussian to the resonance strengths S_{idf} calculated from Eq. (4).

Here, x_q is the fraction of the ions in charge state q, $\sigma_{\mathrm{RR}(2)}(q,E)$ is the RR cross section for recombination to $n=2$, and

$$\sigma_i^{\mathrm{DR}}(q,E) = \sum_d \sum_f S_{idf} G(E-E_{di}) \tag{7}$$

is the total cross section for dielectronic recombination of Kr^{q+} target ions from the initial level i. S_{idf} are the individual resonance strengths Eq. (4) and $G(E-E_{di})$ is the normalized Gaussian that has to be convoluted with S_{idf} for comparison of Eq. (6) to the experimental data. The sums over the intermediate levels d and over the final levels f in Eq. (7) are taken according to the experimental channel-specific cut under investigation. For example, in order to analyze the excitation function for the $n=2-1$ x rays of the KLM resonance, the sums are taken over all the $1s2l3l'$ levels d and over all the $1s^2 3l'$ levels f. In determining the best fit between the experimental and theoretical dielectronic-excitation functions, the relative charge-state balance x_q and the energy width of $G(E-E_{di})$ corresponding to the electron-beam energy width have been treated as independent parameters in Eqs. (6) and (7). In addition, the energy axis was adjusted during the fit procedure to correct for the space charge of the electron beam. The most probable model parameters were found using Poisson statistics and the method of maximum likelihood for the fit of the model to the experimental data [19,20]. As an example, Figs. 2 and 3 show the observed and fitted DR excitation functions for the KLL and KLO resonances, respectively. The background

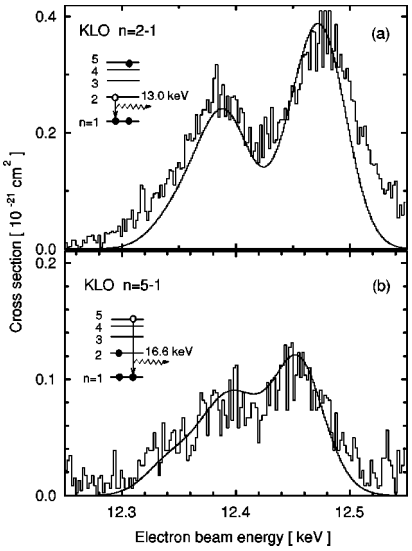

FIG. 3. Comparison between experiment and theory for the channel-specific dielectronic-excitation functions of the *KLO* resonance of highly ionized krypton. Different from the *KLL* resonance, for the *KLO* resonance only the He-, Li-, and Be-like ions were included in the fit procedure. The relative charge-state balance we obtained is $x_{\mathrm{He}}=0.53$, $x_{\mathrm{Li}}=0.37$, and $x_{\mathrm{Be}}=0.10$. (a) and (b), respectively, correspond to the $n=2-1$ and $n=5-1$ x rays at about 13.0 and 16.6 keV. The inset illustrates an energy-level diagram of the stabilizing transition in a He-like ion.

under the dielectronic-recombination resonances from the RR photons was subtracted in each case. For the *KLL* resonance, excellent agreement between experiment and theory can be stated. Note that DR features of B- and C-like ions are observed in addition to the higher charge states. The shape of the *KLL* excitation function is very sensitive to the ionization balance because the resonances for the different charge states [Fig. 2(b)] are well separated from each other. It is worth mentioning that this particular property offers a spectroscopic method for the determination of the charge-state distribution that does not demand analysis of extracted ions. The magnitude of the DR cross section, on the other hand, is quite insensitive to the ionization balance because the cross sections for radiative recombination vary only slightly as a function of the ionization state. While for the *KLL* resonance only the $n=2-1$ x rays occur, for the *KLO* resonance shown in Fig. 3, the $n=2-1$ as well as the $n=5-1$ x rays are observed. For the conditions of Fig. 3, the two branches for the *KLO* resonance approximately differ by a factor of 3. Compared with the *KLL* resonance, the ionization balance for the *KLO* resonance was found to be shifted to higher charge states. This is due to the fact that the fraction of ions that recombine when the beam energy is ramped over the resonance is larger for *KLL* than for *KLO*.

From the comparison of the experimental and theoretical excitation functions around the *KLL*, *KLM*, *KLN*, and *KLO* resonances, we were able to assess the reliability of the dielectronic-recombination data used in the fit procedure. For the experimental excitation functions, we estimate a typical uncertainty (counting statistics) of 5–10%, depending on the resonance under investigation. The principal source of error in calculating the intensity ratio $I_{\mathrm{DR}}/I_{\mathrm{RR}(2)}$ is composed of the theoretical uncertainty in the calculation of the RR cross sections (3% error) and the uncertainty introduced in Eq. (6) due to the fact that we have suppressed the angular corrections (7–10% error). Taking these errors as a basis, for the comparison between experiment and theory, we get an uncertainty interval of 11–16%. Within this limit, there is good overall agreement between the results of the experiment and of the calculation, confirming the dielectronic-recombination data used in the present analysis. Table II displays, for the He-, Li-, and Be-like charge states, the total theoretical DR resonance strengths. It should be noted that the agreement between experiment and theory for the *KLL* and *KLM* resonances is almost perfect. For the weaker resonances, resulting from dielectronic capture into high-*n* levels, the agreement becomes somewhat worse, as is apparent for the *KLO* resonance shown in Fig. 3. A plausible explanation is the limited sensitivity of our measurements, but it is also likely that adding the DR resonances of the B- and C-like ions may reduce the discrepancy.

TABLE II. Total theoretical DR resonance strengths of He-, Li-, and Be-like krypton ions in units of 10^{-20} cm^2 eV. For resonances higher than *KLL*, the channel-specific strengths are given.

Resonance group	Decay channel	Resonance strength Kr^{34+}	Kr^{33+}	Kr^{32+}
KLL	$2\rightarrow1$	54.2	43.9	36.1
KLM	$2\rightarrow1$	21.7	15.2	15.2
	$3\rightarrow1$	8.7	6.9	4.3
KLN	$2\rightarrow1$	8.9	7.1	5.9
	$4\rightarrow1$	3.4	2.0	1.2
KLO	$2\rightarrow1$	4.4	3.5	2.9
	$5\rightarrow1$	1.7	0.9	0.4

In Fig. 4, we present, for several different elements, the total dielectronic-recombination resonance strengths for the He-like *KLn* ($n=2,\ldots,5$) resonance groups. Our results

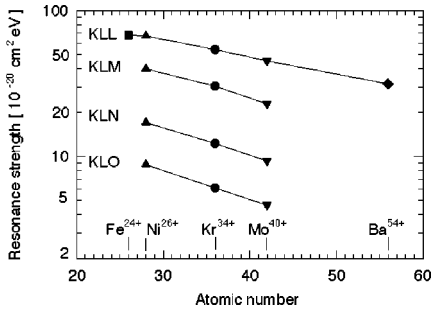

FIG. 4. Total dielectronic-recombination resonance strengths for the *KLn* ($n=2,\ldots,5$) resonance groups of He-like ions. The results for krypton (Kr^{34+}) are acquired in the present investigation. The values for nickel (Ni^{26+}), molybdenum (Mo^{40+}), and barium (Ba^{54+}) are from previously reported EBIT experiments [2]. The iron result (Fe^{24+}) is from another EBIT experiment [21] where individual DR resonance strengths were measured using high-resolution x-ray spectroscopy. The value for the *KLL* resonance strength of iron was obtained by summing over the individual strengths using the data from Tables I and II in Ref. [21]. With the exception of the result for iron, all of the data presented are obtained from a fit procedure of experimental and theoretical DR excitation functions.

TABLE III. Fraction (in %) of counts measured for $n=3-2$, $4-2$, and $5-2$ transitions of the spectator electron, normalized to the $n=2-1$ counts of the stabilizing transition.

Resonance group	Spectator shell	Transition $n=3$-2	$n=4$-2	$n=5$-2	Σ
KLM	3	96			96
KLN	4	13	81		94
KLO	5	10	20	66	96

for krypton (Kr^{34+}) compare well with the trend predicted by the previously reported data for nickel (Ni^{26+}) and molybdenum (Mo^{40+}). Also displayed in Fig. 4 are results for the *KLL* resonance of He-like iron (Fe^{24+}) and barium (Ba^{54+}). It is important to note that the results for iron were obtained with a quite different experimental method allowing to distinguish individual-level resonances. Although this high-resolution technique adds a further level of complexity when compared to the solid-state detector measurements, the data point for iron agrees well with the general trend for the *KLL* resonance strengths.

It remains to discuss the relaxation spectrum, which is generated by the decay of the spectator electron after the $n=2-1$ stabilizing transition has completed the DR process. With the exception of the *KLL* group, each resonance group produces a corresponding relaxation spectrum with x-ray lines extending over a large energy range. Table III summarizes, for the *KLM*, *KLN*, and *KLO* resonances, the measured intensities of the respective $n=3-2$, $4-2$, and $5-2$ transitions normalized to the stabilizing $n=2-1$ transition. It is obvious that the relaxation transitions under consideration can be the result of both direct and multistep decays of the spectator electron to the $n=2$ shell. The data in Table III show that most of the ion relaxation proceeds in one step taking the excited ion directly to the ground state. The x-ray lines originating from these transitions span the energy range from 2 to 3.5 keV. Additionally, it follows from Table III that the total number of counts detected in the relaxation transitions is always less than the intensity of the related $n=2-1$ stabilizing transition. We attribute this result to the nonisotropic x-ray emission in EBIT. A closer look at the individual dielectronic-recombination resonances shows that many of the stabilizing transitions populate (singly excited) states of total angular momentum $J_f=\frac{1}{2}$. The emission from $J_f=\frac{1}{2}$ levels, however, is in any case isotropic independent of the final state and the type of transition. Thus, to the extent that $J_f=\frac{1}{2}$ levels are populated in the DR process, we expect the effect of the directionality for the relaxation transitions to be less significant than for the stabilizing ones. Therefore, the emission intensity actually measured in the relaxation spectrum should be somewhat smaller compared to the $n=2-1$ dielectronic-recombination line. A result, which is also observed in the experiment.

V. CONCLUSIONS

We have investigated the channel-specific dielectronic recombination cross section for the KLn ($n=2,\ldots,5$) series of He-, Li-, and Be-like krypton ions. The measurements employ a technique where the dielectronic recombination is observed by detecting the characteristic x rays emitted in the process. The x-ray data were normalized to the $n=2$ radiative-recombination photons and compared to theory. For this comparison, theoretical values of the DR resonance strengths and the RR cross sections are evaluated from atomic-structure calculations using the HULLAC computer code package. The experimental data were fitted to predicted dielectronic-recombination functions, determining the beam-energy resolution and the ionization balance simultaneously. The agreement between the x-ray data and the modeled dielectronic-excitation functions is better than the estimated uncertainty interval of $11-16\%$.

The experimental approach used for measuring the dielectronic-excitation function opens a way of determining *in situ* by spectroscopic methods the relative charge-state distribution. It appears that the strong *KLL* resonance is ideally suited for this purpose. In the present experiment, for example, up to five charge states (He- to C-like krypton ions) were resolved in the dielectronic-recombination spectrum for this resonance.

The total dielectronic recombination resonance strengths for He-like krypton Kr^{34+} have been compared to previously reported results on Fe^{24+}, Ni^{26+}, Mo^{40+}, and Ba^{54+} showing excellent agreement with the He-like isoelectronic sequence. In addition, our results clearly demonstrate that the decay of a dielectronically excited ion via the higher-energy stabilizing transition is an important process, even if a high-n state is populated in the DR reaction.

A particular aspect of our investigation was the observation of the x-ray emission spectrum from the ion relaxation following an $n=2-1$ stabilizing transition in the dielectronic-recombination process.

ACKNOWLEDGMENT

One of the authors (E. B.) is indebted to the Charles Clore Israel Foundation for support.

[1] C. Biedermann, A. Förster, G. Fußmann, and R. Radtke, Phys. Scr. **T73**, 360 (1997).

[2] D. A. Knapp, R. E. Marrs, M. B. Schneider, M. H. Chen, M. A. Levine, and P. Lee, Phys. Rev. A **47**, 2039 (1993).

[3] A. Bar-Shalom, M. Klapisch, and W.H. Goldstein, The HULLAC Code for Atomic Physics (unpublished).

[4] C. J. Cummings, S. A. Cohen, R. Hulse, D. E. Post, and M. Redi, J. Nucl. Mater. **176&177**, 916 (1990).

[5] M. Bitter, H. Hsuan, C. Bush, S. Cohen, C. J. Cummings, B. Grek, K. W. Hill, J. Schivell, M. Zarnstorff, P. Beiersdorfer, A. Osterheld, A. Smith, and B. Fraenkel, Phys. Rev. Lett. **71**, 1007 (1993).

[6] K. Widmann, P. Beiersdorfer, V. Decaux, R. Elliott, D. Knapp, A. Osterheld, M. Bitter, and A. Smith, Science **66**, 761 (1995).

[7] R.E. Marrs, M.A. Levine, D.A. Knapp, and J.R. Henderson, Phys. Rev. Lett. **60**, 1715 (1988).
[8] B. M. Penetrante, J. N. Bardsley, D. DeWitt, M. Clark, and D. Schneider, Phys. Rev. A **43**, 4861 (1991).
[9] C. Biedermann, R. Radtke, and G. Fußmann, Phys. Rev. A **56**, R2522 (1997).
[10] E. Behar, A. Peleg, R. Doron, P. Mandelbaum, and J. L. Schwob, J. Quant. Spectrosc. Radiat. Transf. **58**, 449 (1997).
[11] M. Klapisch, Comput. Phys. Commun. **2**, 239 (1971).
[12] A. Bar-Shalom, M. Klapisch, and J. Oreg, Phys. Rev. A **38**, 1733 (1988).
[13] M. H. Chen, At. Data Nucl. Data Tables **34**, 301 (1986).
[14] J. H. Scofield, Phys. Rev. A **40**, 3054 (1989).
[15] R. M. Steffen and K. Alder, in *The Electromagnetic Interaction in Nuclear Spectroscopy*, edited by W. D. Hamilton (North-Holland, Amsterdam, 1975), p. 505.
[16] I. C. Percival and M. J. Seaton, Philos. Trans. R. Soc. London, Ser. A **251**, 113 (1958).
[17] M. K. Inal and J. Dubau, J. Phys. B **22**, 3329 (1989).
[18] M. Pajek and R. Schuch, Phys. Rev. A **45**, 7894 (1992).
[19] W. T. Eadie, D. Drijard, F. E. James, M. Ross, and B. Sadoulet, *Statistical Methods of Experimental Physics* (North-Holland/American Elsevier, Amsterdam/New York, 1971).
[20] S. Baker and R. D. Cousins, Nucl. Instrum. Methods Phys. Res. A **221**, 437 (1984).
[21] P. Beiersdorfer, T. W. Phillips, K. L. Wong, R. E. Marrs, and D. A. Vogel, Phys. Rev. A **46**, 3812 (1992).